

## BLOCK PSEUDOSPECTRAL METHODS FOR MAXWELL'S EQUATIONS II: TWO-DIMENSIONAL, DISCONTINUOUS-COEFFICIENT CASE\*

TOBIN A. DRISCOLL<sup>†</sup> AND BENGT FORNBERG<sup>†</sup>

**Abstract.** Block pseudospectral (BPS) methods are examined for Maxwell's equations in two-dimensional inhomogeneous media. For the case of a rectangular strip with a straight-line interface, blocks may be coupled via fictitious points or a generalization of characteristic outflow conditions. The BPS methods generalize to curvilinear strips described by a change of variables. Such strips can conform to interfaces while overlapping with a high-order free-space grid to form a composite grid method. Numerical experiments on strips with dielectrics, lossy materials, perfect conductors, and absorbing layers indicate that the two coupling methods are comparable and accurate with just 3–4 points per wavelength. Full composite examples are included to demonstrate high accuracy and geometric flexibility.

**Key words.** Maxwell's equations, pseudospectral methods, composite grids

**AMS subject classifications.** 65M70, 65M55, 78-08

**PII.** S106482759833320X

**1. Introduction.** In [9] we compared block pseudospectral (BPS) methods for the numerical solution of Maxwell's equations in one dimension, in particular the case where coefficients are discontinuous (i.e., a change of medium). We introduced a new method, based on *fictitious points*, in which blocks are coupled via certain continuity conditions at the block interfaces. In Table 1.1 we compare various methods for the one-dimensional (1D) test problem

$$(1.1) \quad \begin{aligned} \epsilon(x) \frac{\partial E}{\partial t} &= -\frac{\partial H}{\partial x}, \\ \frac{\partial H}{\partial t} &= -\frac{\partial E}{\partial x} \end{aligned}$$

for  $x \in [-1, 1]$ , where

$$(1.2) \quad \epsilon(x) = \begin{cases} 1 & \text{if } x < 0, \\ 4 & \text{if } x > 0. \end{cases}$$

Periodic boundary conditions are imposed to allow the study of long-term behavior. The table shows a snapshot of a propagated pulse and the accuracy of the nonzero eigenvalues of the discrete time differentiation operator. Low-order methods, such as Yee's [24, 26] and finite elements (FE) [3, 4], suffer from strong numerical dispersion unless (typically) at least 10 points per shortest wavelength are used, with 20 or 30 not uncommon [3, 4, 24]. Simply using standard pseudospectral (PS) methods as though the discontinuity did not exist works surprisingly well [12], but the loss of smoothness in the fields destroys the spectral accuracy [20]. A standard spectral

---


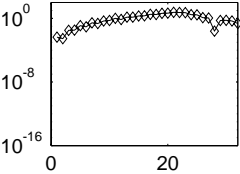
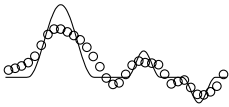
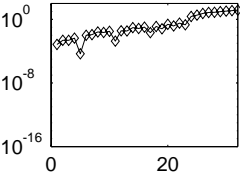
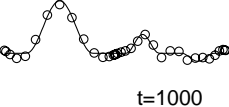
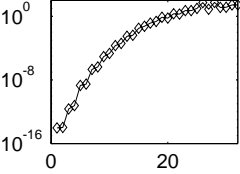
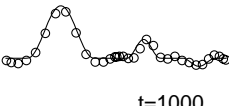
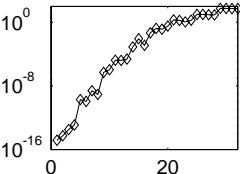
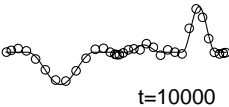
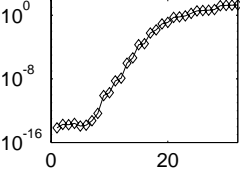
\*Received by the editors January 26, 1998; accepted for publication (in revised form) December 1, 1998; published electronically December 3, 1999.

<http://www.siam.org/journals/sisc/21-3/33320.html>

<sup>†</sup>Department of Applied Mathematics, University of Colorado, Boulder, CO 80309 (tad@colorado.edu, fornberg@colorado.edu). The work of the first author was funded by an NSF postdoctoral research fellowship. Support for the second author was provided by NSF DMS-9706919 and AFOSR.

TABLE 1.1

Summary of methods for 1D test problem (1.1) with discontinuous coefficient (1.2). Each snapshot compares the numerical to the analytical solution for  $E$  at some time. The measured eigenvalues are those of the time-differentiation operator which are in the upper half-plane. All numerical solutions are based on 34 grid points in  $[-1, 1]$ .

Method	Solution snapshot	Eigenvalue accuracy	Comment
Low-order (Yee, FE)	 Yee, t=4		Dispersion errors quickly dominate
Fourier PS	 t=60		Discontinuity degrades spectral accuracy
Characteristic upwinding	 t=1000		Slightly unstable in time
FP(1,0.5)	 t=1000		Comparable to characteristics
FP(4,0.4)	 t=10000		Highest accuracy

element approach, in which Chebyshev grids are coupled via characteristic upwind conditions, is more accurate but slightly unstable in time; the method-of-lines operator has a spectrum extending about  $10^{-4}$  into the right half-plane. The instability occurs at modest wavenumbers and thus would be difficult to filter or dissipate out. (The characteristic coupling here is different and better than that used in [9].) The fictitious

point (FP) method, as introduced in [9], is parameterized by the number of fictitious points used and by the grid clustering (defined as  $\gamma$  in (2.2) below). At the lowest-order coupling, FP(1,0.5), the FP method is slightly more accurate than characteristics and much more stable. With more coupling, FP(4,0.4), the method is even more accurate, as can be seen from the eigenvalues.

In this paper we consider the two-dimensional (2D) linear equations for transverse electric (TE) waves:

$$(1.3a) \quad \epsilon(y) \frac{\partial E_x}{\partial t} = \frac{\partial H_z}{\partial y} - \sigma(y) E_x,$$

$$(1.3b) \quad \epsilon(y) \frac{\partial E_y}{\partial t} = -\frac{\partial H_z}{\partial x} - \sigma(y) E_y,$$

$$(1.3c) \quad \mu \frac{\partial H_z}{\partial t} = \frac{\partial E_x}{\partial y} - \frac{\partial E_y}{\partial x} - \sigma^*(y) H_z.$$

We first present BPS methods for the strip  $S = \{-2 \leq x \leq 2, -1 \leq y \leq 1\}$  with periodic boundary conditions. We choose units so that  $\mu = 1$ . The other material properties are piecewise constant in the regions  $S^- = \{-1 < y < 0\}$  and  $S^+ = \{0 < y < 1\}$  but may be discontinuous at the interfaces  $y = 0$  and  $y = \pm 1$ .

In the  $x$ -direction everything is homogeneous and there are no difficult issues. Computation of the  $y$ -derivatives of  $E_x$  and  $H_z$  across the interface is more troublesome, as these fields can lose smoothness. It is natural to decompose the computational domain into  $S^-$  and  $S^+$  and employ high-order or spectral methods within each subdomain, but then one is faced with the problem of coupling the subdomains.

We shall extend the FP approach to this 2D situation. We will also describe the application of characteristic (upwind) coupling conditions in some detail, as there do not appear to be any references on implementing this for the variety of discontinuous interface situations considered here. In experiments with dielectrics, imperfect conductors, and absorbing layers, the two coupling methods appear to be roughly comparable. Both are acceptably accurate at 3–4 points per wavelength (PPW).

With the rectilinear strip  $S$  described, we will then generalize to curvilinear regions described by a change of variables from  $S$ . Nothing essential changes for either type of BPS coupling. Such a change of variables allows us to simulate a small region about an interface. These interface treatments are part of a larger *composite grid* scheme [8] illustrated in Figure 1. In the free-space “background” of the domain, we use an equispaced, high-order finite difference (FD) method. This offers a good trade-off between high accuracy and geometric versatility. For this purpose the staggered, spatially implicit schemes presented in [13] are especially well suited. Some of the grid points of the background method overlap with thin strips near interfaces, in which a BPS method is used. In the overlapping regions, we use a simple interpolation scheme that connects the different methods. This composite scheme is tested in experiments that demonstrate the method’s high accuracy and geometric flexibility.

## 2. FP method.

**2.1. Interface conditions.** The rectilinear strip is divided into  $S^+$  above the interface and  $S^-$  below it (see Figure 2). To differentiate in  $y$  for  $S^+$ , we use the field values for  $E_x$  and  $H_z$  there plus an extension of those values a small way into  $S^-$ . (Notice that we never need  $\partial_y E_y$ .) A similar extension also occurs for the values in  $S^-$  into  $S^+$ . These extensions occur across both interfaces, at  $y = 0$  and  $y = \pm 1$ .

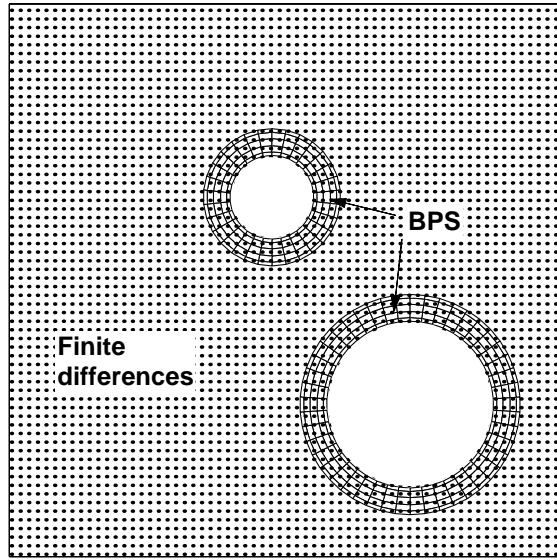


FIG. 1. Composite grid scheme combining a high-order “background” with BPS methods around interfaces.

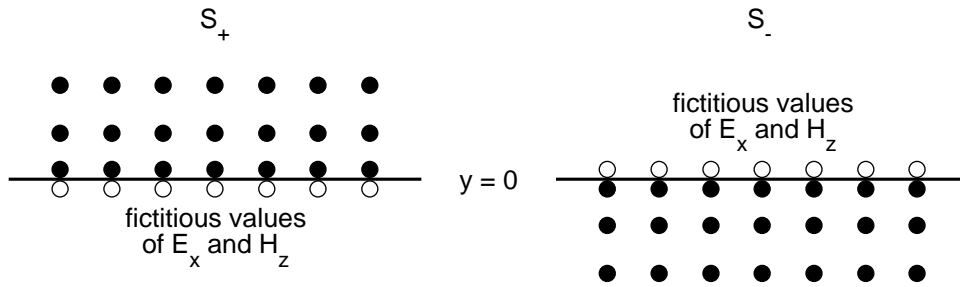


FIG. 2. Schematic representation of FP method. Each subdomain has one layer of fictitious points across the interface. The fictitious values of tangential fields are determined by the physical continuity of those fields at the interface. These fictitiously extended fields have smoothness that is not present in the true fields.

We determine the values of the extensions by enforcing conditions at the interfaces derived from the governing equations.

It is well known [23] that across an interface between transparent media the tangential fields  $E_x$  and  $H_z$  are continuous. Because an interface point has unique values for these fields for all time, we can also conclude the continuity of their time derivatives. Using (1.3a) and (1.3c) we conclude the continuity of

$$(2.1) \quad \begin{aligned} E_x, & \quad \frac{1}{\epsilon} \left( \frac{\partial H_z}{\partial y} - \sigma E_x \right), \\ H_z, & \quad \frac{\partial E_x}{\partial y} - \frac{\partial E_y}{\partial x} - \sigma^* H_z \end{aligned}$$

at the interfaces.

The FP approach rests on the observation that the continuity of the quantities in (2.1) is sufficient to couple the domains. No reference whatsoever need be made to the characteristic form of the governing equations, which is the traditional vehicle for domain coupling. A similar condition for the 1D dielectric case has been proposed before [10], but our generality and implementation appear to be unique.

In principle, we could obtain more accuracy by imposing higher-order conditions derived by taking more time derivatives of  $E_x$  and  $H_z$ , as was done in the 1D case [9]. However, such conditions involve  $x$ -derivatives of these two field components, causing a lateral coupling of all fictitious points and increasing the numerical work substantially. We have observed good results by using only first-order conditions (i.e., those in (2.1)). In doing so, we sacrifice the more uniform grid spacing and consequent larger stable time step as seen in [9]. Because the tangential coupling is relatively weak, it may be possible to fashion efficient iterative methods for higher-order coupling, if deemed important.

In the special case where the material properties are continuous at the interface, the higher-order continuities are equivalent to the continuity of  $E_x$ ,  $H_z$ , and their normal derivatives. These could be quite easily implemented. In light of the 1D case (see Table 1.1), this should improve accuracy substantially. We do not pursue this here, because our main interest is in the discontinuous case.

**2.2. Numerical method.** The field values are stored on a Cartesian-product grid. The grid points are spaced evenly in the  $x$ -direction. In the  $y$ -direction, each domain  $S^+$  and  $S^-$  has a nonuniform, open-ended grid, determined by the number of grid points  $N$  and parameter  $\gamma$  according to

$$(2.2) \quad \frac{j - \frac{1}{2}}{N} = \int_{-1}^{y_j} c_\gamma (1 - y^2)^{-\gamma} dy, \quad c_\gamma = \frac{\Gamma(3/2 - \gamma)}{\sqrt{\pi} \Gamma(1 - \gamma)},$$

for  $j = 1, \dots, N$ . These points, which lie in  $(-1, 1)$  by the choice of  $c_\gamma$ , are scaled to the interval  $(-1, 0)$  or  $(0, 1)$  as appropriate. The parameter  $\gamma$  controls the amount of grid clustering near the ends of the interval. As discussed in [9], one must classically choose  $\gamma = 0.5$  as  $N \rightarrow \infty$ . However, for modest  $N$ , one may choose  $\gamma < 0.5$ , leading to more uniform grids.

We use Fourier PS differentiation in  $x$  and the FP technique for differentiation in  $y$ . Consider first the interface  $y = 0$ . Along each vertical grid line we place on each side of the interface one fictitious point for each of  $E_x$  and  $H_z$ . (The exact locations of the fictitious points are unimportant.) The four unknown field values are determined by discretization of the four conditions in (2.1).

The mechanics are represented schematically in Figure 2. Over the physical grid points in  $S^+$  and the fictitious point with  $y < 0$ , we construct FD weights of maximum (PS) order, as described in [12], to find interpolated function and  $y$ -derivative values at  $y = 0$ . These weights apply to both the known and unknown values of  $E_x$  and  $H_z$  to produce  $E_x$ ,  $H_z$ ,  $\partial_y E_x$ , and  $\partial_y H_z$  at  $y = 0$ . In addition, we use the known values of  $\partial_x E_y$  in  $S^+$  to extrapolate to  $y = 0$ . (We choose  $\gamma = 0.5$  to avoid instabilities in the extrapolation.)

Thus we have values “from above” at  $y = 0$  for all the quantities appearing in (2.1). We set these equal to values determined similarly “from below.” The result, after rearrangement, is a  $4 \times 4$  linear system for the fictitious field values at each  $x$ -grid location. The right-hand side of the system depends linearly on the physical field values in  $S^+$  and  $S^-$ . The algebraic details are similar to those spelled out for the 1D case in [9]. Both the system and the right-hand matrices are identical for every

vertical grid line and invariant in time, so they need be computed just once. The work involved in constructing and solving these systems is insignificant compared to the work needed to compute derivatives in the interior of the domains.

Because of the periodicity in  $y$ , the process must be repeated for the interface at  $y = \pm 1$ . One then has physical values for  $E_x$  and  $H_z$  in  $S^+$  and one fictitious value apiece above and below the interfaces. We use all the values to compute the  $y$ -derivatives in  $S^+$ . The situation in  $S^-$  is identical.

**3. Characteristic coupling.** The dominant method of coupling spectrally discretized domains in hyperbolic problems is to use characteristics. Following [6], we group characteristic methods into two categories: *correctional* and *differential*. In the correctional method one collocates the differential equation independently in each domain during a time step, including at the interface. Characteristics are used after each time step to reconcile the interface quantities to ensure upwinding [15, 25]. In the differential method, derivatives are first computed independently, but characteristics are used to reconcile values of time derivatives at the interface [6, 14, 19, 22].

There does not seem to be a clear winner between these alternatives. The correctional method retains the order of accuracy of Runge–Kutta time integrators, but the stability restriction on the time step may become much more restrictive [7, 21]. The differential technique, on the other hand, may reduce the order of accuracy of Runge–Kutta methods if time and space are simultaneously resolved, but there appear to be no serious stability consequences [21].

For the current problem, either method can be used. In this paper we consider only the differential method. Because the coupling takes place for the time derivatives, a standard ODE package can be used for the time integration; this is not possible with the correctional approach. We will set the tolerance of the ODE solver to make time errors negligible, so order of accuracy in time is not an issue.

We now describe some details of the characteristic upwinding (CU) method we use for the TE waves described by (1.3). We write the equations in vector form:

$$(3.1) \quad \partial_t w + A(\partial_x w) + B(\partial_y w) = Fw,$$

where

$$w = \begin{bmatrix} E_x \\ E_y \\ H_z \end{bmatrix}, \quad A = \begin{bmatrix} 0 & 0 & 0 \\ 0 & 0 & 1/\epsilon \\ 0 & 1 & 0 \end{bmatrix}, \quad B = \begin{bmatrix} 0 & 0 & -1/\epsilon \\ 0 & 0 & 0 \\ -1 & 0 & 0 \end{bmatrix}, \quad F = \begin{bmatrix} -\sigma & 0 & 0 \\ 0 & -\sigma & 0 \\ 0 & 0 & -\sigma^* \end{bmatrix}.$$

Our interface is normal to  $y$ , so we diagonalize  $B$ :

$$(3.2) \quad B = V^{-1}\Lambda V, \quad V = \begin{bmatrix} -\sqrt{\epsilon} & 0 & 1 \\ 0 & 1 & 0 \\ \sqrt{\epsilon} & 0 & 1 \end{bmatrix}, \quad \Lambda = \begin{bmatrix} 1/\sqrt{\epsilon} & 0 & 0 \\ 0 & 0 & 0 \\ 0 & 0 & -1/\sqrt{\epsilon} \end{bmatrix}.$$

First, suppose that  $\epsilon$  is the same in both domains. Away from the interface, we can write (3.1) as

$$(3.3) \quad \partial_t w = V^{-1}[-\Lambda V(\partial_y w) - VA(\partial_x w) + VFw].$$

At an interface point, we will use the upward-going characteristic quantity from below

and the downward-going quantity from above. Thus we define

$$(3.4) \quad V_u = [-\sqrt{\epsilon} \quad 0 \quad 1], \quad \Lambda_u = \frac{1}{\sqrt{\epsilon}},$$

$$(3.5) \quad V_d = [\sqrt{\epsilon} \quad 0 \quad 1], \quad \Lambda_d = -\frac{1}{\sqrt{\epsilon}}.$$

Because  $E_y$  does not propagate in the  $y$ -direction, it has a different role from the other variables. In what follows we will need

$$(3.6) \quad \tilde{w} = \begin{bmatrix} E_x \\ H_z \end{bmatrix}, \quad \tilde{V} = \begin{bmatrix} -\sqrt{\epsilon} & 1 \\ \sqrt{\epsilon} & 1 \end{bmatrix}, \quad \tilde{V}_u = [-\sqrt{\epsilon} \quad 1], \quad \tilde{V}_d = [\sqrt{\epsilon} \quad 1],$$

obtained by deleting  $E_y$  from consideration.

Using superscripts  $+$  and  $-$  to denote quantities computed from  $S^+$  and  $S^-$ , we generalize (3.3) to

$$(3.7) \quad (\partial_t \tilde{w})^0 = \begin{bmatrix} \tilde{V}_u \\ \tilde{V}_d \end{bmatrix}^{-1} \begin{bmatrix} -\Lambda_u V_u (\partial_y w)^- - V_u A (\partial_x w)^- + V_u F w^- \\ -\Lambda_d V_d (\partial_y w)^+ - V_d A (\partial_x w)^+ + V_d F w^+ \end{bmatrix},$$

where the zero superscript means the reconciled value at  $y = 0$ . We have yet to specify how to compute  $(\partial_t E_y)^0$ . Because  $H_z$  has a single, well-defined value along the interface, we use the unique value of  $\frac{1}{\epsilon} (\partial_x H_z)^0$ .

Suppose now that  $\epsilon$  jumps from  $\epsilon^-$  in  $S^-$  to  $\epsilon^+$  in  $S^+$ . The characteristic variables and speeds are now also discontinuous. However, they continue to have the same form, and there is still one in each direction, with  $E_y$  being neutral. We propose to generalize (3.7) to

$$(3.8) \quad (\partial_t \tilde{w})^0 = \begin{bmatrix} \tilde{V}_u^- \\ \tilde{V}_d^+ \end{bmatrix}^{-1} \begin{bmatrix} -\Lambda_u V_u^- (\partial_y w)^- - V_u^- A^- (\partial_x w)^- + V_u^- F^- w^- \\ -\Lambda_d V_d^+ (\partial_y w)^+ - V_d^+ A^+ (\partial_x w)^+ + V_d^+ F^+ w^+ \end{bmatrix},$$

where the superscripts have been applied to the matrices to indicate their values in  $S^+$  or  $S^-$ . Retracing through the definitions, this becomes

$$(3.9) \quad \left( \partial_t \begin{bmatrix} E_x \\ H_z \end{bmatrix} \right)^0 = \frac{1}{\sqrt{\epsilon^+} + \sqrt{\epsilon^-}} \begin{bmatrix} -1 & 1 \\ \sqrt{\epsilon^+} & \sqrt{\epsilon^-} \end{bmatrix} \times \begin{bmatrix} (\partial_y E_x)^- - \frac{1}{\sqrt{\epsilon^-}} (\partial_y H_z)^- - (\partial_x E_y)^- + \sqrt{\epsilon^-} \sigma^- E_x^0 - (\sigma^*)^- H_z^0 \\ (\partial_y E_x)^+ + \frac{1}{\sqrt{\epsilon^+}} (\partial_y H_z)^+ - (\partial_x E_y)^+ - \sqrt{\epsilon^+} \sigma^+ E_x^0 - (\sigma^*)^+ H_z^0 \end{bmatrix}.$$

We have used superscript zero for undifferentiated fields, as they have unique values at the interface.

Computing  $(\partial_t E_y)^0$  is less clear now, because whereas  $(\partial_x H_z)^0$  is again unique, the value of  $\epsilon$  is not. We instead maintain two values of  $E_y$  at an interface point, in accordance with

$$(3.10) \quad \partial_t (E_y^\pm) = \frac{1}{\epsilon^\pm} (\partial_x H_z)^0.$$

Since these fields are in general related by a frequency-dependent ratio [23], computing both seems reasonable.

The numerical procedure is to first compute spatial derivatives of the fields independently within  $S^+$  and  $S^-$  to get the one-sided values appearing in (3.9). One then finds the reconciled values of the time derivatives of  $E_x$  and  $H_z$ , keeping two values for  $E_y$  at the interface. Thus the time derivatives of each field are known at every grid point, and the field values can be advanced by an ODE integrator as in the method of lines.

Note that (3.8) and (3.10) is not the only generalization of (3.7); indeed, a different one was used in [9]. It can be shown, however, that (3.8) and (3.10) hold exactly for an arbitrary reflected and transmitted plane wave solution. Equation (3.9) agrees with the description of characteristic “ghosts” in [18]. Furthermore, the numerical evidence in section 7 also supports the use of our generalization.

In the CU method, we are applying first-order continuity equations on the fields *after* computing their derivatives. By contrast, in the FP approach the conditions are applied to the fields *simultaneously* with computing their derivatives.

**4. Extensions.** We make a few remarks on how to apply both coupling procedures to two other important situations: perfect conductors and reflectionless absorbers.

Suppose we solve in the domain  $S^+$  and wish to simulate a perfect electrical conductor at  $y = 0$ . In the characteristic method, we simply impose  $E_x = 0$  at a boundary point and simulate Maxwell’s equations for  $E_y$  and  $H_z$ . In the FP method, we use a single fictitious point with  $y < 0$  at which we need values of  $E_x$  and  $H_z$ . At the interface,  $E_x$  and  $\partial_t E_x$  are zero, so the conditions  $E_x = 0$  and  $\partial_y H_z = 0$  are sufficient to determine fictitious values.

There is great interest in absorbing perfectly matched layers (PML) for simulation of radiation out of a domain. The most widely known PML, due to Berenger [5], requires a nonphysical splitting of the magnetic field that enlarges the system from three to four partial differential equations. It has been shown [1] that the Berenger PML is only weakly well posed and may in fact be prone to instability in practice.

An alternative model, called TD-LM and based on Lorentz materials [27], is strongly well posed. Furthermore, it can be written using a supplemental ODE rather than a new PDE [2]. Assuming  $S^-$  is the absorbing layer and  $S^+$  is free space with  $\epsilon = \mu = 1$ , the TD-LM equations are

$$\begin{aligned} (4.1a) \quad & \frac{\partial E_x}{\partial t} = \frac{\partial H_z}{\partial y} - \rho(y)E_x, \\ (4.1b) \quad & \frac{\partial E_y}{\partial t} = -\frac{\partial H_z}{\partial x} + \rho(y)E_y - P, \\ (4.1c) \quad & \frac{\partial H_z}{\partial t} = \frac{\partial E_x}{\partial y} - \frac{\partial E_y}{\partial x} - \rho(y)H_z, \\ (4.1d) \quad & \frac{\partial P}{\partial t} = -\rho(y)P + \rho(y)^2 E_y, \end{aligned}$$

where  $\rho(y)$  is a loss parameter that is zero outside  $S^-$ . Thus in  $S^+$ ,  $P \equiv 0$  and the system reduces directly to the standard Maxwell (1.3). Continuity of  $E_x$  and  $H_z$  is still assured for all frequencies and incidence angles, so the FP method still imposes the continuity of the quantities in (2.1) at the interface, with  $\rho$  replacing  $\sigma$ . Likewise, the new variable  $P$  does not propagate, so there is no need to involve it in characteristic quantities. As with  $E_y$ ,  $P$  may be discontinuous, so we maintain dual values  $P^\pm$  at the interface.



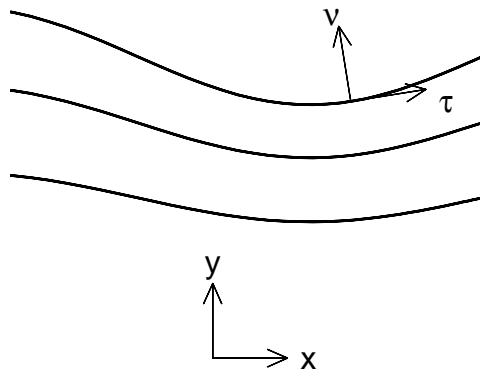


FIG. 3. Change of variables from normal coordinates  $(\tau, \nu)$  to physical coordinates  $(x, y)$ .

It is pointed out in [2] that a jump in  $\rho$  at the interface causes discontinuities in  $E_y$  and  $P$ , and the authors recommend avoiding this situation. On the other hand, activating  $\rho$  continuously or smoothly leaves the fields with more smoothness, but certain waves in the absorber may actually grow. We have found (see section 7) that the reflection coefficients are acceptably small even in the discontinuous case, when the interface is implemented as described above. In particular, maintaining the one-sided values of  $E_y$  and  $P$  appears to be successful.

**5. Variable coefficients.** The solution of problems on rectilinear strips is of little intrinsic interest. To begin building toward a practically useful method, we introduce a change of variables into the formulation.

Let  $(\tau, \nu)$  be the variables of the strip  $S$ , and let  $(x(\tau, \nu), y(\tau, \nu))$  be a smooth change of variables to physical coordinates. We shall continue to assume that  $S$  is periodic in the  $\tau$ -direction, but not in the  $\nu$ -direction. The strip variables are intended to represent “tangential” and “normal” directions in physical space, and the line  $\nu = 0$  should map to an interface in physical space. See Figure 3.

Define the metrics

$$(5.1) \quad \begin{aligned} h_\tau^2 &= \left( \frac{\partial x}{\partial \tau} \right)^2 + \left( \frac{\partial y}{\partial \tau} \right)^2, \\ h_\nu^2 &= \left( \frac{\partial x}{\partial \nu} \right)^2 + \left( \frac{\partial y}{\partial \nu} \right)^2. \end{aligned}$$

Define also the fields

$$(5.2) \quad \begin{aligned} E_\tau &= \frac{1}{h_\tau} \left[ \frac{\partial x}{\partial \tau} E_x + \frac{\partial y}{\partial \tau} E_y \right], \\ E_\nu &= \frac{1}{h_\nu} \left[ \frac{\partial x}{\partial \nu} E_x + \frac{\partial y}{\partial \nu} E_y \right]. \end{aligned}$$

Then it is a simple matter to show that the TE Maxwell’s equations in physical space

$(x, y)$  transform in  $S$  to

$$\begin{aligned}
 (5.3) \quad \epsilon \frac{\partial E_\tau}{\partial t} &= \frac{1}{h_\nu} \frac{\partial H_z}{\partial \nu} - \sigma E_\tau, \\
 \epsilon \frac{\partial E_\nu}{\partial t} &= -\frac{1}{h_\tau} \frac{\partial H_z}{\partial \tau} - \sigma E_\nu, \\
 \frac{\partial H_z}{\partial t} &= \frac{1}{h_\nu h_\tau} \left[ \frac{\partial}{\partial \nu} (h_\tau E_\tau) - \frac{\partial}{\partial \tau} (h_\nu E_\nu) \right] - \sigma^* H_z.
 \end{aligned}$$

These equations change the coupling conditions of the BPS methods only a little. In the FP method, we have continuity of the tangential fields  $E_\tau$  and  $H_z$  and their time derivatives at  $\nu = 0$ . The only substantial change in the method is introduced by the variation of the metrics (5.1) along the interface. The  $4 \times 4$  linear system that needs to be solved will have different entries at each point along  $\nu = 0$ .

To extend characteristic coupling to the variable-coefficient case, it is best to use the primitive variables

$$w = \begin{bmatrix} h_\tau E_\tau \\ h_\nu E_\nu \\ H_z \end{bmatrix}.$$

With this, the matrices analogous to (3.2) that describe the characteristic variables and speeds in the  $\nu$ -direction are

$$V = \begin{bmatrix} -h_\tau \sqrt{\epsilon} & 0 & 1 \\ 0 & 1 & 0 \\ h_\tau \sqrt{\epsilon} & 0 & 1 \end{bmatrix}, \quad \Lambda = \begin{bmatrix} (h_\nu \sqrt{\epsilon})^{-1} & 0 & 0 \\ 0 & 0 & 0 \\ 0 & 0 & -(h_\nu \sqrt{\epsilon})^{-1} \end{bmatrix}.$$

With these it is a straightforward matter to generalize (3.7) to variable coefficients. As in the FP case, the only serious new element is the variation of the particular linear combination that must be used at each interface point.

**6. Interpolation for composite grids.** At this point, certain geometries (say, thin-layered media) could be immediately fit into the BPS framework. The final step toward a more general utilization of BPS methods is to incorporate them into a broader domain-decomposition framework, such as the overlapping, composite grid approach illustrated in Figure 1. We envision the BPS method being used in thin layers about material interfaces.

The background grid overlaps all the BPS grids. To complete the method, we need to specify how information is transferred between them. To make the description as clear as possible, we reduce to a 1D situation, which captures all the essential features. Let the finite-difference grid range over  $[-1, \delta]$ , overlapping with a PS grid in  $[0, 1]$ . We define a *blending function*  $b(x)$  that smoothly rises from 0 at  $x = 0$  to 1 at  $x = \delta$ . For example,  $b(x) = (1 - \cos(\pi x/\delta))/2$ .

The idea behind our method is that each grid should independently advance one time step. The values then need to be reconciled in such a way that values near the edge of a grid are replaced by interpolation from the other grid. The “trust” from one grid to the other is transferred gradually in a way described by the blending function, in order to avoid artificial Gibbs-type discontinuities.

To be more explicit about the 1D case, let  $f_1$  and  $f_2$  be vectors of function values in the FD and PS grids, respectively. By the “overlap points” of a grid we mean

the points of that grid that are in the overlap region  $[0, \delta]$ . We define two restriction matrices,  $R_1$  and  $R_2$ , such that  $R_i f_i$  is the vector of values at the overlap points of grid  $i$ . We also have interpolation matrices  $P_{12}$  and  $P_{21}$ , such that  $P_{ij} f_j$  is the interpolation of values from grid  $j$  to the overlap points of grid  $i$ . Finally, we have diagonal matrices  $B_1$  and  $B_2$  whose diagonals are the evaluation of  $b(x)$  at the overlap points in each grid.

We update the overlap values according to

$$(6.1) \quad \begin{aligned} R_1 f_1^{(\text{new})} &= B_1(P_{12} f_2^{(\text{old})}) + (I - B_1)R_1 f_1^{(\text{old})}, \\ R_2 f_2^{(\text{new})} &= (I - B_2)(P_{21} f_1^{(\text{old})}) + B_2 R_2 f_2^{(\text{old})}. \end{aligned}$$

We have left the order of accuracy of interpolation unspecified. The precise value is unimportant, so long as it is consistent with the order of the differentiation calculations.

Returning to the context of a 2D composite-grid method, one must map the FD points that lie inside a BPS region to the  $(\tau, \nu)$ -coordinates of the strip. Likewise, one must determine the coordinates of BPS grid points in physical space. Interpolation from a grid is done in that grid's native coordinate system. Blending is based on the value of  $(\tau, \nu)$  at an overlap point.

Because we interpolate to an interval (in two dimensions, a region) rather than a boundary point (edge), we do not need to be overly concerned about the "boundary closure" chosen for the implicit FD grid. Nor do we need to find characteristic variables to ensure outflow. All the coordinate mapping, interpolation, and blending needs to be done just once before time stepping, and each interpolatory correction consumes a small amount of time compared to spatial derivative evaluations.

## 7. Numerical experiments.

**7.1. The BPS method on strips.** The FP, CU, and Yee methods were implemented and tested in MATLAB. Each of the test problems below was given the same initial condition. With  $r$  as the distance from a point to  $(0, 0.5)$ , the initial fields are given by

$$H_z(x, y) = \begin{cases} \frac{1}{32}(10 + 15 \cos(\frac{\pi r}{0.3}) + 6 \cos(\frac{2\pi r}{0.3}) + 3 \cos(\frac{3\pi r}{0.3})) & \text{if } r \leq 0.3, \\ 0 & \text{otherwise,} \end{cases}$$

$$E_x(x, y) = (y - 0.5)H_z(x, y),$$

$$E_y(x, y) = -xH_z.$$

This arrangement creates a radially symmetric pulse with leading peak and trailing trough. In a medium with unit wave speed, the amplitude of the Fourier component with wavelength about 0.17 has fallen to 1% of the maximum over the whole spectrum. We use this wavelength (when adjusted to the slowest medium in an experiment) as the basis for determining points per wavelength (PPW).

Time integration for the BPS methods is done with MATLAB's built-in ode113 using an error tolerance of  $10^{-8}$ . Hence all the errors seen should be due to spatial discretization. The Yee method uses second-order leapfrog time stepping, with a very small Courant number to minimize time error.

**Test 1: Two dielectric materials.** In this test the material parameters are

$$\begin{aligned} \epsilon^+ &= 1, & \sigma^+ &= 0, & (\sigma^*)^+ &= 0, \\ \epsilon^- &= 4, & \sigma^- &= 0, & (\sigma^*)^- &= 0. \end{aligned}$$

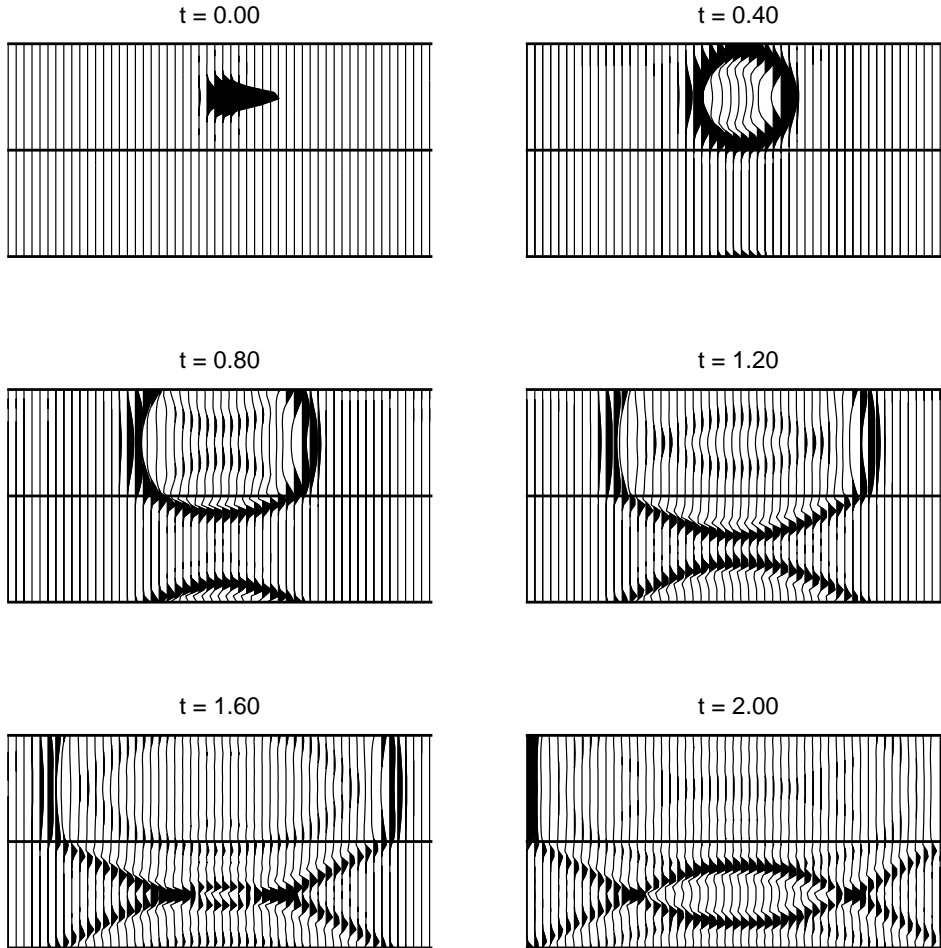


FIG. 4. Snapshots of the solution to the two-dielectric problem for the FP method with 3 PPW.

To achieve 3 PPW, we use a  $144 \times 36$  grid in  $S^-$  and a  $144 \times 27$  grid in  $S^+$  for the BPS methods. These numbers give 3 PPW in the slow medium; the extra resolution in the fast medium was found to be necessary for stability of the FP method. The Yee method has a fixed global resolution of  $144 \times 72$ . To get grids for other PPW requirements, we round off multiples of these values.

In Figure 4 we show snapshots of the time history of the magnetic field  $H_z$  up to  $t = 2$  for the FP method with 3 PPW. The reflected and transmitted wavefronts are clearly seen and no errors are visible. In Figure 5 we compare the BPS solutions at  $t = 2$  to Yee solutions at various PPW. More revealing are the errors, which are presented in Figure 6. The FP and CU methods at 6 PPW agree with each other to an order of magnitude better than with any of the other solutions, so we use CU-6 as the exact solution. Here we can clearly see that even at 32 PPW, Yee's method is less accurate than the BPS methods. The overall accuracy of Yee here is limited by the interior discretization rather than the interface. The maximum error in Yee-32 is about three times that of FP-4 and CU-4, so equivalent accuracy should be reached at about  $\sqrt{3} \cdot 32 \approx 56$  PPW. Based on our fairly naive implementations, the CPU

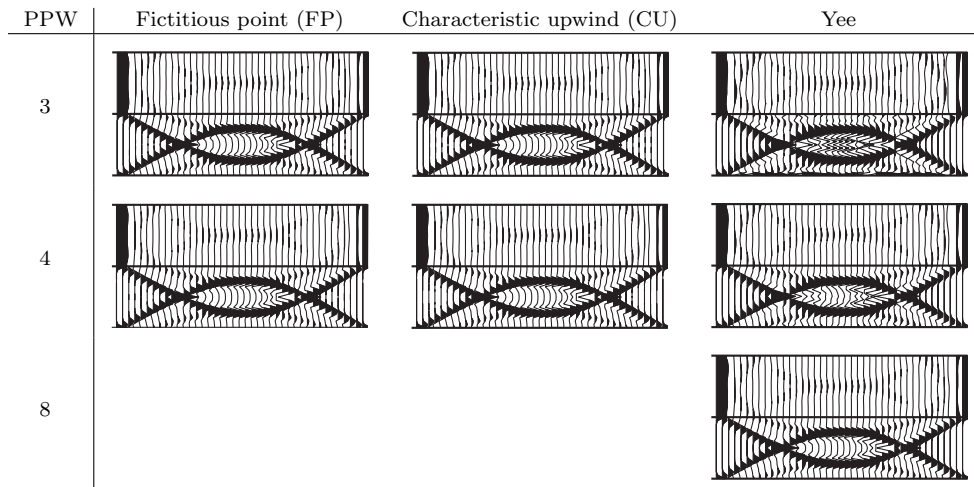


FIG. 5. Solutions at  $t = 2$  for the dielectric problem. Errors are seen more clearly in Figure 6.

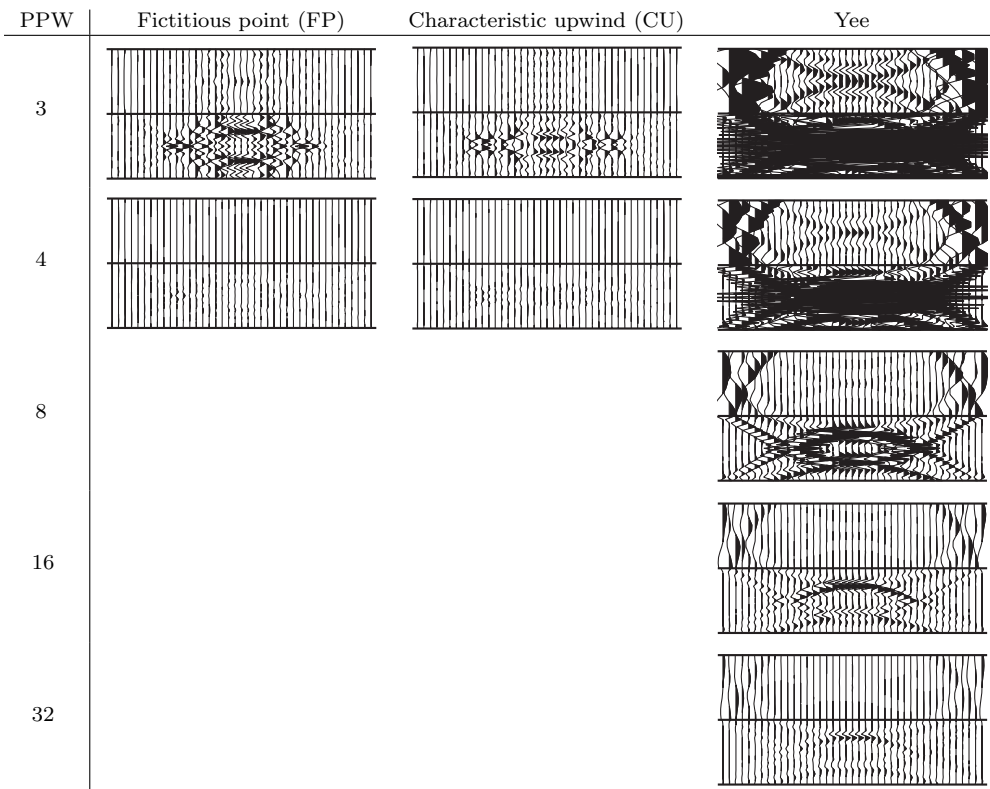


FIG. 6. Errors at  $t = 2$  for the dielectric problem. As an indication of the scale, the maximum error in the case of CU-4 is about 0.001; the maximum of the solution is about 0.23.

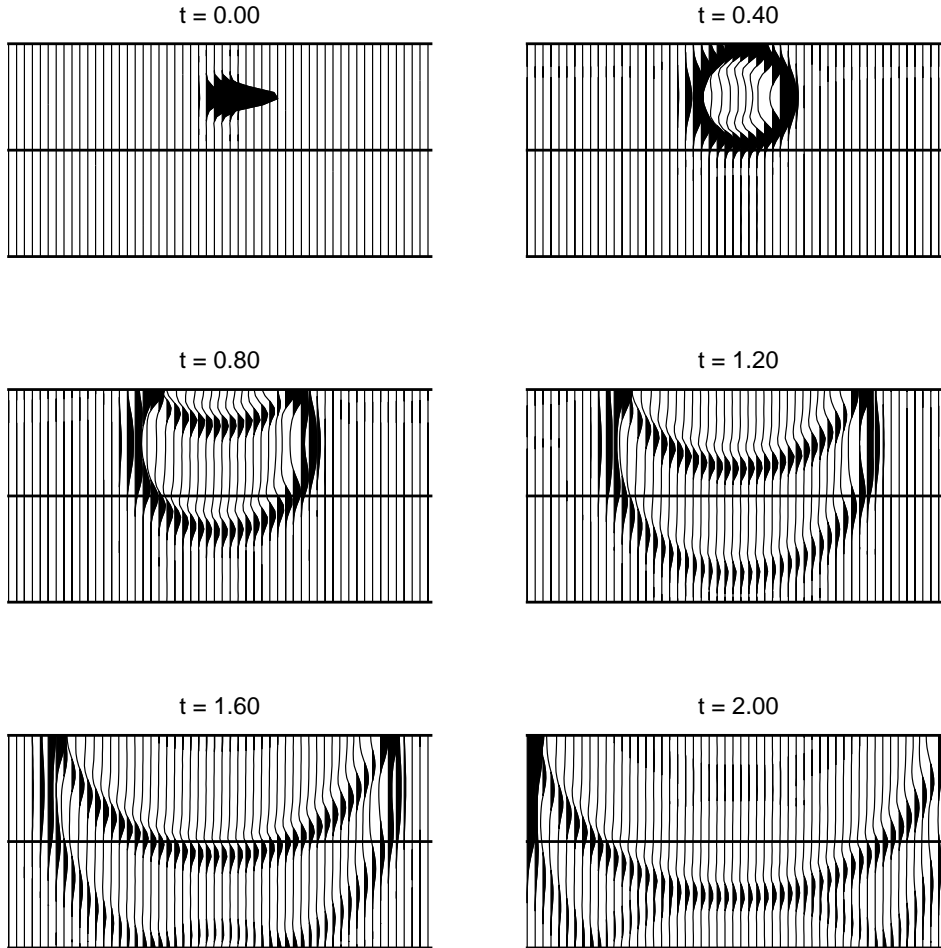


FIG. 7. Snapshots of the solution to the lossy-medium problem using the FP method with 3 PPW.

cost of Yee-56 would be more than 50 times that of FP-4 or CU-4, and the storage requirements would be almost 200 times greater. This experiment was for a relatively short time interval; the dispersive disadvantages of Yee’s method can be expected to grow with time.

**Test 2: Lossy material.** Here we test a material with finite conductivity, as well as nonperiodic boundaries in the  $y$ -direction. The material properties are

$$\begin{aligned} \epsilon^+ &= 1, & \sigma^+ &= 0, & (\sigma^*)^+ &= 0, \\ \epsilon^- &= 1, & \sigma^- &= 2, & (\sigma^*)^- &= 0. \end{aligned}$$

At  $y = \pm 1$  we place a perfect electrical conductor.

Figure 7 shows the results for the FP method with 3 PPW (a  $72 \times 18$  grid in each domain). Reflection from the perfect conductors is clearly evident, as is damping of the wave in the lossy medium. There are also small reflections into  $S^+$  from the interface, but the amplitudes are too small to be seen here. Results for the CU method are visually indistinguishable from those in Figure 7.

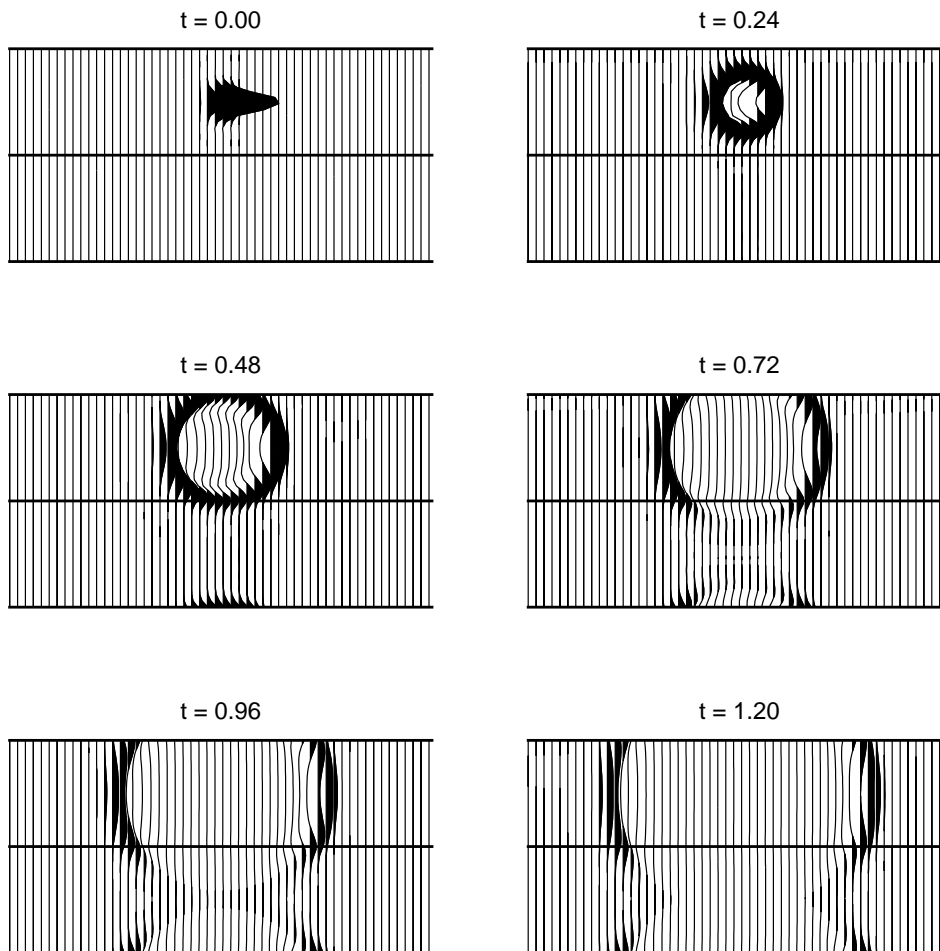


FIG. 8. Snapshots of the solution to the TD-LM absorber problem using the FP method with 3 PPW.

**Test 3: TD-LM absorber.** The material properties are

$$\begin{aligned} \epsilon^+ &= 1, & \rho^+ &= 0, \\ \epsilon^- &= 1, & \rho^- &= 10. \end{aligned}$$

We use a  $72 \times 18$  grid in each subdomain to achieve 3 PPW in the BPS methods, and  $72 \times 36$  overall for the Yee method.

Snapshots of the solution using the FP method are displayed in Figure 8. The absorption of the wave is clear, and no reflected wave is visible.

We can find the reflected wave by running an identical simulation in free space (without the absorber) and subtracting off this solution in  $S^+$ . The results of doing this at  $t = 1.2$  are shown in Figure 9. The amplitude of the reflected wave is taken as the maximum in  $S^+$  of the difference of solutions. This number is normalized by 0.15, which is the approximate amplitude of the wave when it encounters the boundary of the absorber. Both BPS methods achieve good convergence as the resolution increases (with CU being slightly better). By comparison, the Yee method yields rather large

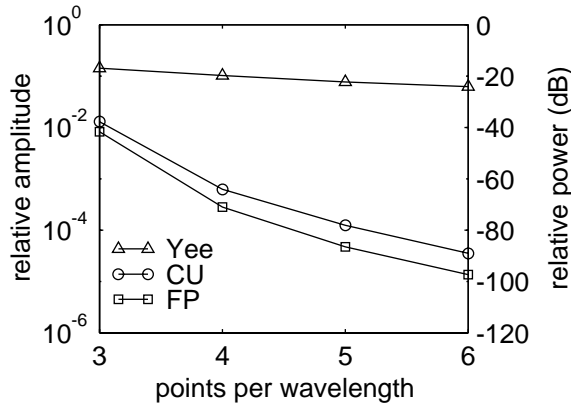


FIG. 9. Reflection amplitude and power for TD-LM absorbing layer. The results are relative to the incident wave.

reflections; in [27] 50 PPW were required to achieve a reflection of  $-100$  dB.

**7.2. Composite grids.** We now consider FP BPS methods as part of a larger composite grid strategy. Our first test geometry is that shown in Figure 1. The background FD method is the sixth order, staggered, tridiagonally implicit scheme presented in [13]. A pulsed plane wave of amplitude 1 is propagated from the left. All the time stepping is by a fourth-order Runge–Kutta method with a small, fixed step size.

In the first case, the entire domain is free space. This is to test the fundamental concepts of variable coefficients and interpolation. An additional ring is used inside each of the circles of Figure 1 so that each BPS method consists of two layers. The FD grid is also continued into the circles. The resolution of the FD grid is about 3.6 PPW, and the BPS grids are at about 2 PPW azimuthally and 3 PPW radially. Blending depends on the depth of penetration into the annular layers. Figure 10 shows snapshots of the numerical solution. Accuracy at the final time shown is about 5.5% in the max norm, or 4.9% in the discrete 2-norm.

We now change the circular regions to perfect conductors. Figure 1 shows the precise discretization used, including grid point locations; only one layer per BPS grid is needed. Resolution is the same as in the previous case. We do not have an exact solution for this situation, so we rely on the accuracy of the free-space problem and the clear visual plausibility of Figure 11. (Note that the last frame has an artificial reflection from the outer domain boundary.)

To further demonstrate the versatility of the method, we use a nonperiodic BPS method in Figures 12 and 13. The FD grid is again at 3.6 PPW and the PS grids are set at about 3 PPW. The interpolation is based on a 2D blending function in the rectangle, which has an inclination of  $70^\circ$ . In the first case of free-space propagation, the final error is about 5.2% in 2-norm and 4.9% in max norm. The second case has a perfectly conducting plate that extends across part of the BPS interface. We believe these results can be extended to more general regions with corners.

We emphasize that no artificial damping has been added to any of the test cases. The underlying numerical methods were found to be naturally stable.

**8. Summary.** We have presented two approaches to coupling BPS methods at a discontinuous interface: one based on fictitious points, the other on characteristics.



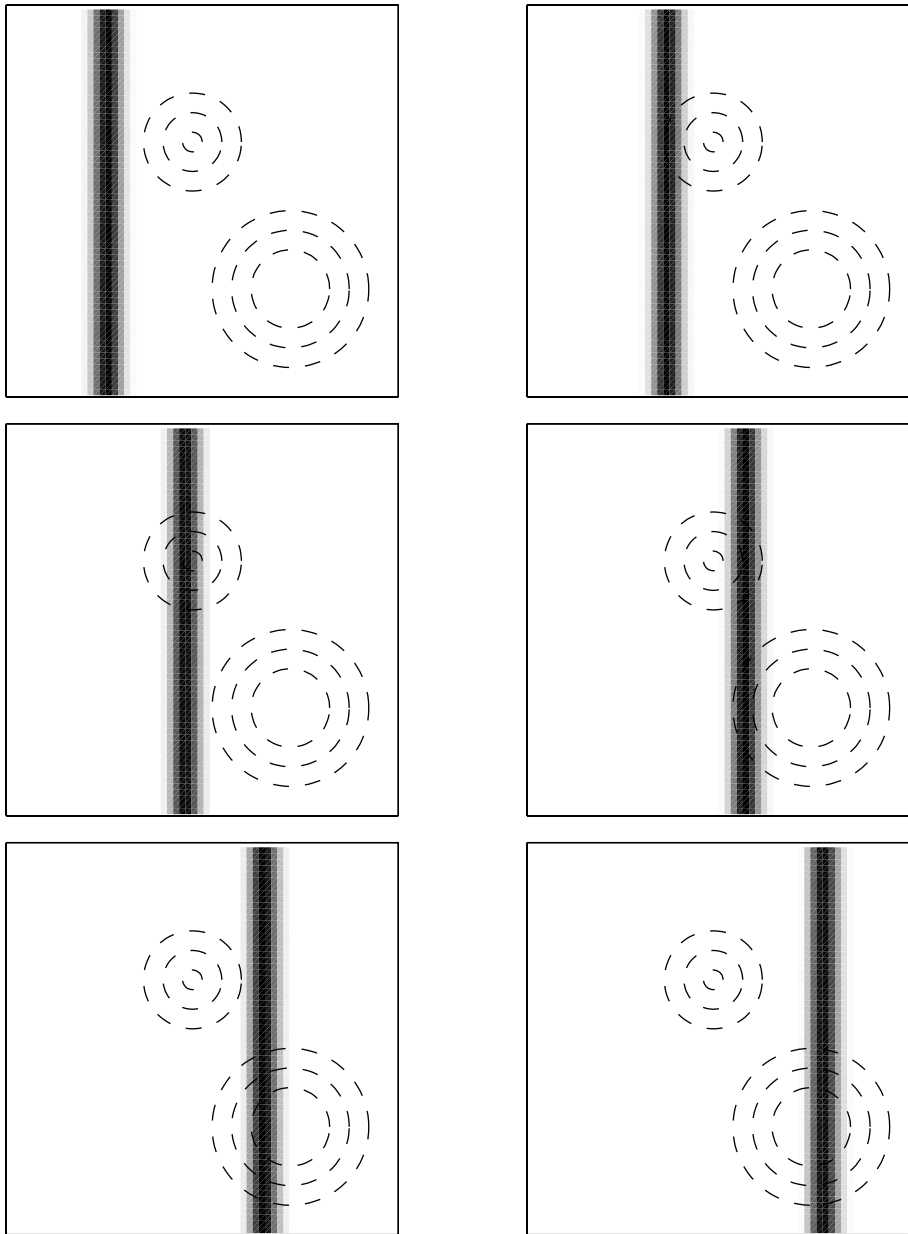


FIG. 10. Propagation of a plane wave in free space, using the composite grid method. Dashed lines show the boundaries of BPS blocks.

The approaches are mutually exclusive. Their differences are summarized in Table 8.1. For the test cases we have considered, the two techniques appear to have comparable accuracy, far superior to that available from low-order methods. Either BPS method should be easily adaptable to three dimensions, or other linear systems.

The FP method, which imposes the correct first-order continuity on the fields before numerical differentiation, is slightly more complex to implement. Because equa-

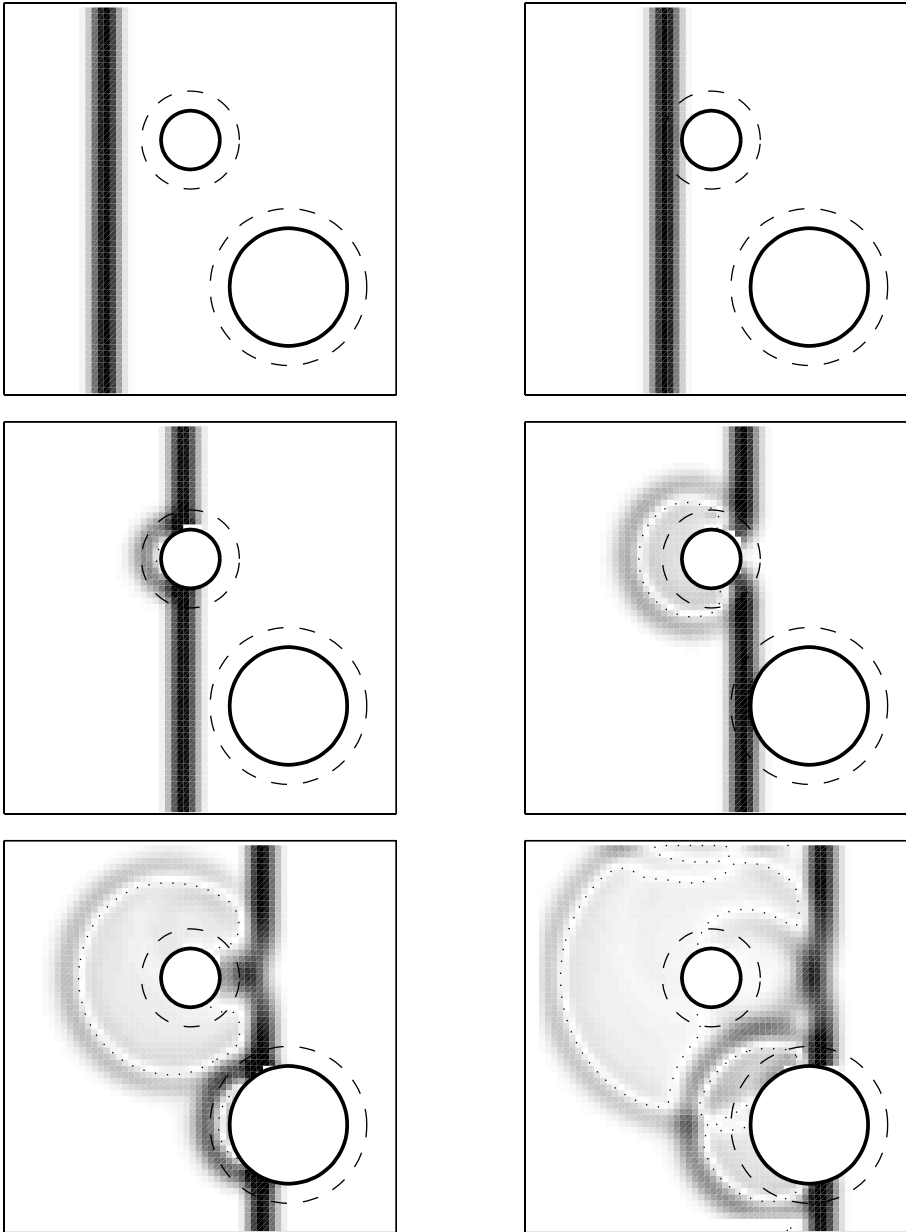


FIG. 11. Scattering from two perfectly electrical conducting cylinders, using the composite grid method. Shading indicates magnitude of the magnetic field (black is maximum). The dotted contours show the zero level.

tions are not collocated at the interface, there is no ambiguity in time integration. Moreover, one can stagger the grids as in Yee's scheme to improve accuracy [11, 17]. In one dimension, this has led to eigenvalues that are an order of magnitude more accurate, although the stable time step becomes smaller. At interfaces with continuous coefficients, the method becomes much simpler, and additional fictitious points can be added effortlessly to enhance accuracy significantly.

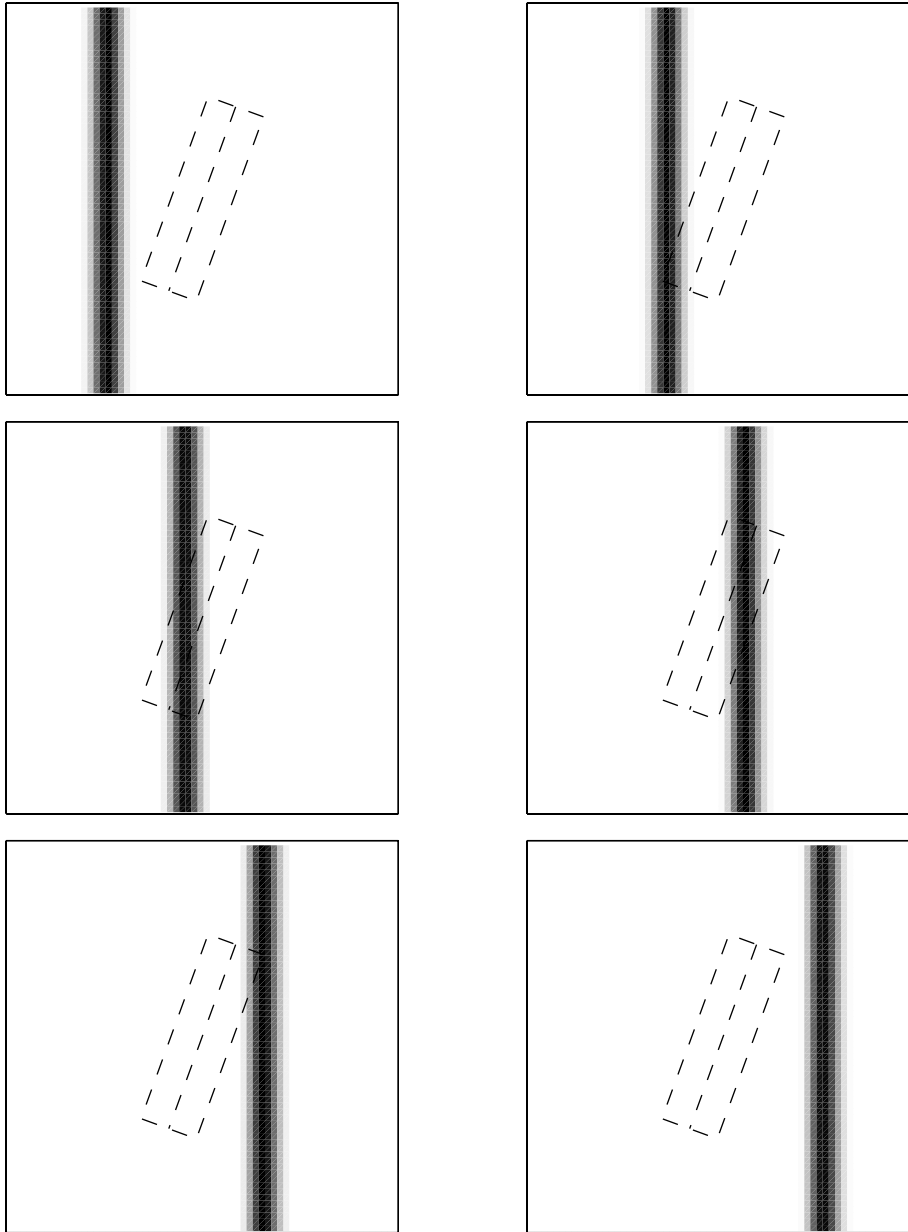


FIG. 12. *Free-space propagation with the composite method in another geometry.*

The characteristic coupling method, which enforces first-order correctness after differentiation, is somewhat easier and perhaps more familiar to implement. However, the location of grid points at the interface requires a choice in time integration that entails serious trade-offs. We do not see how such a method could exploit staggered grids. An additional issue that our tests avoided arises at subdomain corners, where the direction of “outward” flow is not clear.

A desirable improvement would be to allow the grids to change in the tangential

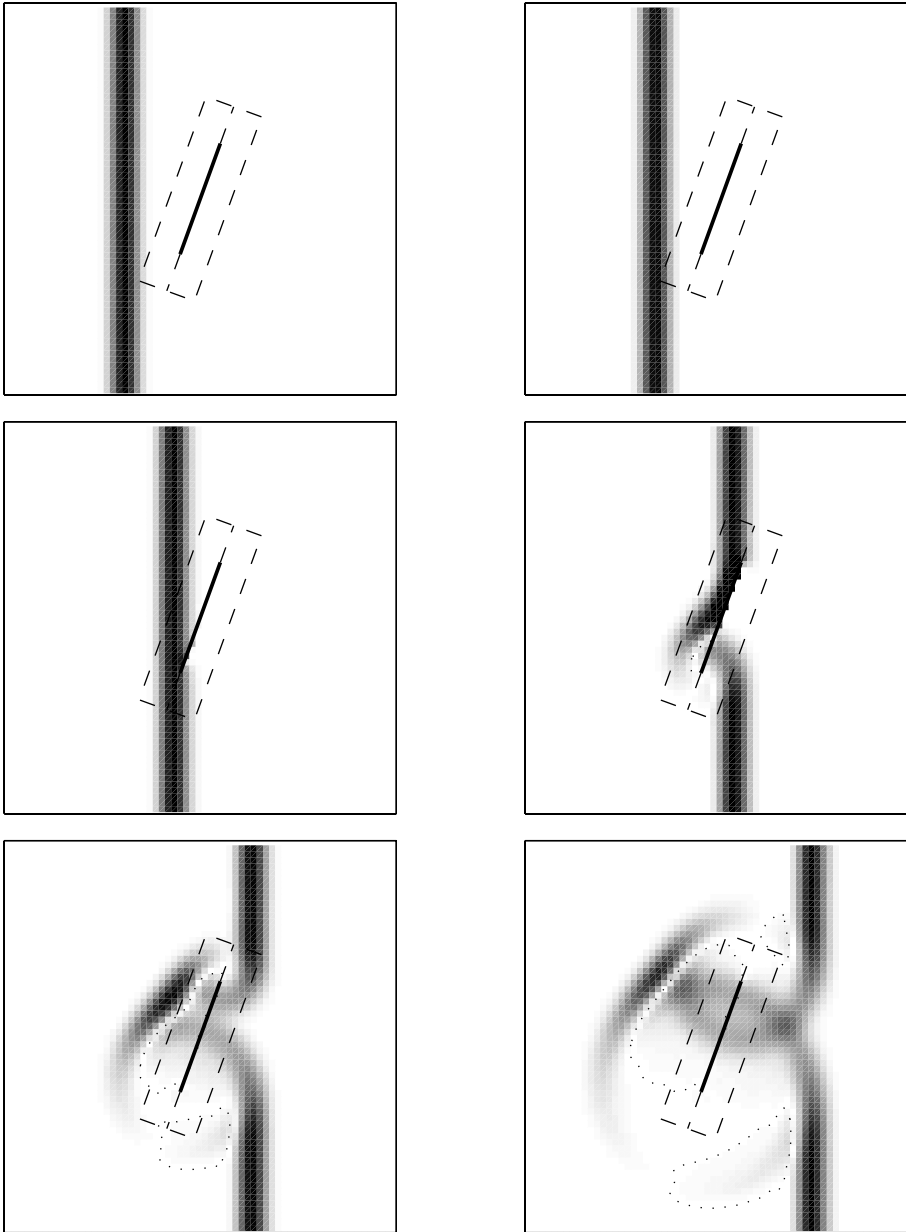


FIG. 13. Scattering from a perfectly conducting plate (solid line), located along part of the BPS interface.

direction across the interface [3, 4, 16] to allow more natural resolutions on each side. It may be possible to use a projection-type method to do this, as in [16].

We see the BPS methods as accurate simulations of near-interface dynamics. For problems in complex geometry, an equispaced high-order FD method operating in bulk space can be overlapped with mapped BPS grids and linked by interpolation. We have successfully demonstrated this concept in geometries that would prove challenging to

TABLE 8.1  
*Comparison of BPS coupling methods.*

	PF	CU
First-order continuity of fields	Yes	Yes
Higher-order continuity possible	Yes	No
Collocates equations at interface	No	Yes
Allows staggering of grid points	Yes	No
Special treatment required at corners	No	Yes

low-order finite differences or globally spectral methods.

**Acknowledgment.** We thank Morten Bjørhus for a valuable discussion on the issues regarding time integrators for CU methods.

#### REFERENCES

- [1] S. ABARBANEL AND D. GOTTLIEB, *A mathematical analysis of the PML method*, J. Comput. Phys., 134 (1997), pp. 357–363.
- [2] S. ABARBANEL AND D. GOTTLIEB, *On the construction and analysis of absorbing layers in CEM*, Appl. Numer. Math., 27 (1998), pp. 331–340.
- [3] F. ASSOUS, P. DEGOND, AND J. SEGRÉ, *Numerical approximation of the Maxwell equations in inhomogeneous media by a  $P^1$  conforming finite element method*, J. Comput. Phys., 128 (1996), pp. 363–380.
- [4] A. BAMBERGER, R. GLOWINSKI, AND Q. H. TRAN, *A domain decomposition method for the acoustic wave equation with discontinuous coefficients and grid change*, SIAM J. Numer. Anal., 34 (1997), pp. 603–639.
- [5] J.-P. BERENGER, *A perfectly matched layer for the absorption of electromagnetic waves*, J. Comput. Phys., 114 (1994), pp. 185–200.
- [6] M. BJØRHHUS, *The ODE formulation of hyperbolic PDEs discretized by the spectral collocation method*, SIAM J. Sci. Comput., 16 (1995), pp. 542–557.
- [7] M. H. CARPENTER, D. GOTTLIEB, S. ABARBANEL, AND W. S. DON, *The theoretical accuracy of Runge–Kutta time discretizations for the initial-boundary value problem: A study of the boundary error*, SIAM J. Sci. Comput., 16 (1995), pp. 1241–1252.
- [8] G. CHESHIRE AND W. D. HENSHAW, *Composite overlapping meshes for the solution of partial differential equations*, J. Comput. Phys., 90 (1990), pp. 1–64.
- [9] T. A. DRISCOLL AND B. FORNBERG, *A block pseudospectral method for Maxwell’s equations: I. One-dimensional case*, J. Comput. Phys., 140 (1998), pp. 1–19.
- [10] E. FACCIOLI, A. QUARTERONI, AND A. TAGLIANI, *Spectral multidomain methods for the simulation of wave propagation in heterogeneous media*, in Domain Decomposition Methods in Science and Engineering, Sixth International Conference on Domain Decomposition, Como, Italy, A. Quarteroni, J. Periaux, Y. A. Kuznetsov, and O. B. Widlund, eds., Contemporary Math. 157, AMS, Providence, RI, 1994, pp. 447–455.
- [11] B. FORNBERG, *High-order finite differences and the pseudospectral method on staggered grids*, SIAM J. Numer. Anal., 27 (1990), pp. 904–918.
- [12] B. FORNBERG, *A Practical Guide to Pseudospectral Methods*, Cambridge University Press, Cambridge, UK, 1996.
- [13] B. FORNBERG AND M. GHRIST, *Spatial finite difference approximations for wave-type equations*, SIAM J. Numer. Anal., to appear.
- [14] P. HANLEY, *A strategy for the efficient simulation of viscous compressible flows using a multidomain pseudospectral approach*, J. Comput. Phys., 108 (1993), pp. 153–158.
- [15] D. A. KOPRIVA, *Computation of hyperbolic equations on complicated domains with patched and overset Chebyshev grids*, SIAM J. Sci. Statist. Comput., 10 (1989), pp. 120–132.
- [16] D. A. KOPRIVA, *A conservative staggered-grid Chebyshev multidomain method for compressible flows. II. A semi-structured method*, J. Comput. Phys., 128 (1996), pp. 475–488.
- [17] D. A. KOPRIVA AND J. H. KOLIAS, *A conservative staggered-grid Chebyshev multidomain method for compressible flows*, J. Comput. Phys., 125 (1996), pp. 244–261.
- [18] I. LIE, *Interface conditions for heterogeneous domain decomposition: Coupling of different hyperbolic systems*, in Domain Decomposition Methods in Science and Engineering: Sixth International Conference on Domain Decomposition, Como, Italy, A. Quarteroni, J. Periaux,

- Y. A. Kuznetsov, and O. B. Widlund, eds., Contemporary Math. 157, AMS, Providence, RI, 1994, pp. 469–476.
- [19] I. LIE, *Multidomain solution of advection problems by Chebyshev spectral collocation*, SIAM J. Sci. Comput., 9 (1994), pp. 39–64.
- [20] E. LUO AND H.-O. KREISS, *Pseudospectral vs. finite difference methods for initial value problems with discontinuous coefficient*, SIAM J. Sci. Comput., 20 (1998), pp. 148–163.
- [21] D. PATHRIA, *The correct formulation of intermediate boundary conditions for Runge–Kutta time integration of initial-boundary value problems*, SIAM J. Sci. Comput., 18 (1997), pp. 1255–1266.
- [22] A. QUATERONI, *Domain decomposition methods for systems of conservation laws: Spectral collocation approximations*, SIAM J. Sci. Statist. Comput., 11 (1990), pp. 1029–1052.
- [23] J. R. REITZ, F. J. MILFORD, AND R. W. CHRISTY, *Foundations of Electromagnetic Theory*, Addison–Wesley, Reading, MA, 1979.
- [24] A. TAFLOVE, *Computational Electrodynamics: The Finite-Difference Time-Domain Method*, Artech House, Boston, 1995.
- [25] B. YANG, D. GOTTLIEB, AND J. S. HESTHAVEN, *Spectral simulations of electromagnetic wave scattering*, J. Comput., Phys., 137 (1997), pp. 1–15.
- [26] K. S. YEE, *Numerical solution of initial boundary value problems involving Maxwell's equations in isotropic media*, IEEE Trans. Antennas Prop., 14 (1966), pp. 302–307.
- [27] R. W. ZIOLKOWSKI, *Time-derivative Lorentz material model-based absorbing boundary condition*, IEEE Trans. Antennas Prop., 45 (1997), pp. 1530–1535.